The coupled effects of bending and torsional flexural modes of a high-speed train car body on its vertical ride quality

Vahid Bokaeian[a], Mohammad Ali Rezvani[a,*], Robert Arcos[b]

[a] *School of Railway Engineering, Iran University of Science and Technology, Tehran, Islamic Republic of Iran.*

[b] *Acoustical and Mechanical Engineering Laboratory. Universitat Politècnica de Catalunya. Spain.*

Abstract

This study is focused on the effects of bending and torsional flexural modes of the car body on the ride quality index of a high-speed train vehicle. The Euler-Bernoulli beam model is used to extract an analytical model for a high-speed train vehicle car body in order to investigate its bending and torsional flexural vibrations. The rigid model includes a car body, two bogie frames and four wheelsets such that, each mass has three degrees of freedom including vertical displacement, pitch motion, and roll motion. The results obtained with the proposed analytical model are compared with experimental measurements of the car body response of a Shinkansen high-speed train. Moreover, it is determined that the bending and torsional flexural modes have significant effects on the vertical acceleration of the car body, particularly in the 9 Hz to 15 Hz frequency range. Furthermore, the ride quality index is calculated according to the EN 12299 standard and it is shown that the faster the train the more affected is the ride quality by the flexural modes. In addition, the effect of coherence between two rail irregularities (the right and the left rails) on the results of the simulation is investigated. The results conclude that if the irregularities are completely correlated the torsional flexural mode of the car body does not appear in the response. Also, the first bending flexural mode in such cases is more excited compared with the partially correlated or uncorrelated rail irregularities. Therefore, the ride quality index in completely correlated cases are higher than other cases.

Keywords: Flexible vibration of car body, Ride quality index, Vertical vibration of high speed train, Interacting vibration modes.

1. Introduction

In recent decades, increasing the speed of trevel has become more attractive in the rail transport industry as a means to maintain the industry's status in transportation. Japan's Shinkansen is the first high-speed train in the world that reached 200 km/h in 1964. In 2007, the French high-speed train TGV achieved a speed of 574 km/h, breaking the speed record for conventional high-speed trains (based on wheel-rail contact). Japan's Maglev (derived from Magnetic Levitation) has also reached 620 km/h. Today, the efficiency and economic benefits of high-speed train transportation are proven. It is shown that some flexural modes of the car body are similar to the flexural modes of a free-free beam [1] and if the weight of the car body is reduced, there is the possibility to excite the flexural modes in the frequency range relevant for passenger comfort, based on the EN 12299:2009 [2] standard (4 to 20 Hz). In other words, if the weight of the car body is reduced, the effect of flexural modes become more important in point of view of passengers ride comfort. Thus, in such cases, it is necessary to investigate the effect of flexural modes of the car body on the ride comfort of passengers.
Capitani and Tibaldi (1989) [3] offered an active suspension system to reduce car body flexural vibrations. Hac et al. (1996) [4] proposed two methods to reduce the bending vibrations of the car body based on an active secondary suspension system using *modal control* approach and an active dynamic absorber, respectively. Foo and Goodall (2000) [5] proposed a method for reducing the bending vibrations of the car body using an active secondary suspension system by applying a classical control method using *skyhood damping*. Carlbom (2000) [6] investigated the effect of flexible vibrations on the ride quality parameters and shown that the flexibility of the

*Corresponding author
Email address: rezvani_ma@iust.ac.ir (Mohammad Ali Rezvani)

car body must be considered in order to predict the vertical ride quality. Hansson et al. (2004) [7] investigated the reduction of bending vibrations of the car body using piezoelectric elements in order to convert the bending flexural vibration energy to electrical energy which can dissipate by shunt circuit. They applied this method to a 1:5 scaled model of a Shinkansen vehicle. Later on, Takigami and Tomioka (2008) [8], applied this method to a full-scale commuter car. Schandl et al. (2007) [9] applied a feedback control method by using piezoelectric as actuators that were installed on the floor of the car body. Schirrer and Kozek (2008) [10] presented a method for reducing the bending vibrations by adding an actuator to the car body and its active control. Zhou et al. (2009)[11] investigated the effect of flexible bending vibrations on a passenger train and they concluded that increasing the vehicle speed needs higher car body stiffness in order to avoid exciting bending flexural vibration of the car body. Sugahara et al. (2009) [12, 13], in two separate studies, reduced the bending vibrations of the car body. They started by controlling the stiffness of the primary and secondary suspension systems and then by controlling damping of the primary suspension. Orvnas (2010) [14] compared the different active and passive methods of reducing the vertical vibrations of the car body. Tomioka and Takigami (2010) [15] reduced the bending vibrations using the dynamic interaction between the bogies and the car body. They reported that there is a dynamic interaction between longitudinal vibrations of bogies and bending flexural vibration of the car body. Therefore, the first mode of bending flexural vibration of the car body can be attenuated by adjusting the stiffness of the traction rod such that, the bogies act as a dynamic vibration absorber. Kamada et al. (2010) [16] proposed to use an active vibration control by combining linear and piezoelectric actuators to reduce the vibrations of lightweight car bodies. The subject flexible and rigid vibrations were reduced by piezoelectric and linear actuators, respectively. Gong et al. (2013) [17] proposed a method to reduce the flexural car body vibrations using a dynamic absorber with investigating the *wheelbase filtering* and *bogie spacing filtering* effects on the vertical acceleration response of the car body. Escalona et al. (2013) [18] investigated the structural flexibility of railway vehicles and discussed different modelling methods for structural flexibility in railroad vehicles. Sun et al. (2016) [19] used modal sensitivity optimization to improve the modal frequency of the car body. This method is based on the thickness optimization of the car body frame in various longitudinal locations according to the ride quality index. The vertical bending frequency is increased from 9.70 to 10.60 Hz by this method. Graa et al. (2016) [20] studied the effects of the passenger position, loading of the train and its speed on the ride comfort of the passengers. They showed that the ride comfort is affected by the train speed and the position of the passenger more than other parameters. Masoomi and Jalili (2017) [21]investigated the effect of the rail irregularity classification and train speed on the ride quality index with considering the normal wheel-rail contact nonlinearity. They concluded that the rail irregularity affects the vertical acceleration more than the train speed. Dumitriu (2017) [22] investigated the effect of tuning the passive element in the suspension system on the flexural vibrations of the car body. Huang et al. (2018) [23] investigated the effect of car body mounted equipment on the bending flexural vibration of a high-speed train. It is shown that the stiffness, damping, mass and the position of the installed equipment have significant effects on the flexural vibration of the car body. Also, they showed that the flexural vibration can be suppressed significantly by optimizing the related stiffness, damping, mass, and the equipment position.

The motivation for this study came from the fact that all previous studies and efforts were focused to act on the first bending mode of the car body vibrations, whereas it is known that, usually, the frequency of the first torsional mode of the car body is close to the frequency of the first bending mode [6, 17]. Therefore, there is the possibility of exciting the first torsional mode of the car body due to roll motion. Hence, it is vital to know the effect of torsional flexural vibration on the ride quality index. In the present research, a Shinkansen high-speed train (series 100) with aluminum alloy car body is modelled using a combined rigid and flexible model in which the effects of the flexible modes on each other is negligible. Hence such modes are decoupled and each flexible mode is considered as a system degree of freedom. This can be interpreted into the concept that the effect of coupling between the flexible modes are ignored. The rigid multibody system includes the car body, two bogies, and four wheelsets. The considered degrees of freedom for the car body and the bogies are related to vertical, pitch and roll motions. For the wheelsets, only the degrees of freedom related to vertical and roll motions are considered. The flexibility of the car body is included by modeling it as a continuous Euler-Bernoulli beam that takes into account bending and torsional deformations. In addition, the normal contact between the wheels and the rail is modeled by a linear hertz theory. Then, the equations are transformed to the frequency domain to be solved analytically. Obviously, the proposed method of solution is preferable over other available methods such as the FEM methods. Based on the results, it is observed that, in the center of the wagon, the vertical ride quality is influenced only by the first flexural bending mode, and the first mode of torsional and second mode of bending were not observed. But, with increasing the distance from the center of the wagon in the transverse and longitudinal direction, the effects of the first torsional and the second bending modes appear. It is also observed that at some particular speeds, the negative effect of flexible modes on the ride quality index increases. In addition, the effect of correlation between the irregularities of the right and the left rails on the roll motion of the car body is studied.

2. Modeling

2.1. Flexural motion equations

To investigate the effect of torsional and bending flexural car body vibrations, it is considered that the car body is a free-free Euler-Bernoulli beam. The bending vibrations of a beam with a cross-sectional area A, density ρ, structural damping coefficient C_i, and bending rigidity EI are described equation (1) [24].

$$EI\frac{\partial^4 v(x,t)}{\partial x^4} + \rho_b A_b \frac{\partial^2 v(x,t)}{\partial t^2} + C_i \frac{\partial v(x,t)}{\partial t} = -f_{sfr}\delta(x-x_f) - f_{sfl}\delta(x-x_f) - f_{srr}\delta(x-x_r) - f_{srl}\delta(x-x_r) \quad (1)$$

where f_{sfr}, f_{sfl}, f_{srr} and f_{srl} are the forces induced by the secondary suspensions (represented by the first subindex s) to the car body. The second and the third subindices represent the front (f) or the rear (r) wheelset and the left (l) or the right (r) wheel, respectively. The bending modes of an unsupported beam can be written as

$$X_n(x) = \cos\beta_n x + \cosh\beta_n x - \frac{\cosh\beta_n L - \cos\beta_n L}{\sinh\beta_n L - \sin\beta_n L}(\sinh\beta_n x + \sin\beta_n x) \quad (2)$$

where β_n are the values of β that solve the equation

$$\cos\beta L \cosh\beta L = 1 \quad (3)$$

Furthermore, the equation of torsional vibrations of the beam with a torsional moment J, a shear modulus G is as follows [24].

$$\rho J\frac{\partial^2 \phi(x,t)}{\partial t^2} - GK\frac{\partial^2 \phi(x,t)}{\partial x^2} = m_t(x,t) \quad (4)$$

$m_t(x,t)$ is the torsional moments which is applied on the car body by the secondary suspensions. The coefficient K is a torsional constant. Separating the variables, the shape of the torsional modes of the free-free beam can be obtained by using equation (5).

$$X_{n\phi}(x) = \cos\frac{n\pi}{L}x \quad (5)$$

Takigami and Tomioka (2007) [1] obtained the car body flexural modes of a Shinkansen train through stationary and running tests. Their results show the appearance of two bending modes and one torsional mode of the car body in the range of frequencies between 9 Hz and 16 Hz. Figure 5 on article [1] shows the mode shapes and the related frequencies on the corresponding modes. Mode (A) in Figure 5 presents the behavior of the right and the left side beams that are located under the floor that deform vertically in counter-phases. Since shearing deformation of the cross-section of the car body is observed in this mode, it is called the shearing mode [1]. The modes (B) and (C) are similar to the bending and torsion modes of a simple beam, respectively. In the modes (D1) and (D2), both the roof and the floor have vibration shapes that are similar to the second bending mode of a beam combined with a small torsional motion. On the other hand, only mode (D) is identified and is presented in Figure 5(b) and the modes (D1) and (D2) seem to be coupled [1]. Therefore, the car body is assumed as a flexural and torsional beam with two bending modes at the natural frequencies of 9.84 Hz and 15.12 Hz and a torsional mode with a natural frequency of 13.42 Hz. The natural frequencies for the model are obtained by using a free-free beam model for its 1st vibration mode with mechanical properties that are different from the ones in its 2nd mode. Therefore, the car body is not considered as a free-free beam for the entire range of frequency. It is modeled as a free-free beam around 9.84 Hz and 15.12 Hz. The 2nd natural bending frequency at 15.12 Hz is force fed to the model to comply with the results from Takigami and Tomioka (2007)[15]. It is shown by Takigami and Tomioka (2007)[15] that the Shinkansen high-speed vehicle car body behaves like the first bending mode of a free-free beam around 9.84 Hz and also behaves like the second bending mode of a free-free beam around 15.12 Hz. Essentially, it is not practical to replace a car body with a beam for all the frequency range of interest. Thus, there isn't any beam model of a car body with specific parameters (such as E, I, ρ, m, etc.) that its first and second bending modes coincide precisely with the car body's bending modes. Therefore, in this study, the car body is modeled by two free-free beams around 9.84 Hz and 15.12 Hz so that the first and the second bending modes of the beams match with the related modes of the car body, respectively. Based on the modal analysis of a Shinkansen train that is reported by Tomioka and Takigami (2007)[15], a flexible torsional mode at 13.42 Hz was found and presented. This mode is similar to the first

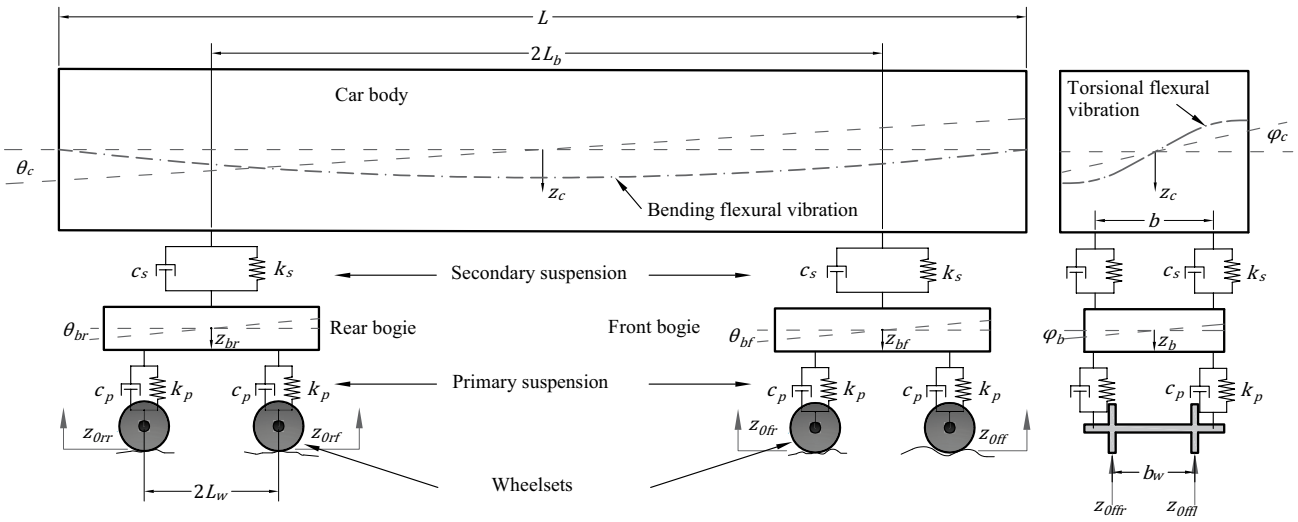

Fig. 1: Schematic view of vehicle.

twisting mode of a free-free beam. Therefore, the car body is considered as a free-free beam under torsional vibration that happens at around 13.42 Hz. This is used to simulate the first flexural-torsional mode of the car body in this research.

2.2. Combined rigid and flexural motion equations

In this section the combined rigid and flexural motion equations of a car body with three degrees of freedom are obtained. Figure 1 shows a schematic view of the vehicle. It is assumed that the car body and each bogie frame have 3 degrees of freedom of rigid body motion, consisting of vertical motion, pitch motion, and roll motion. Flexible body motion is also considered for the car body, as defined in previous section. The wheelsets are considered to be rigid bodies with two degrees of freedom including the vertical and the roll motions. Furthermore, the normal contact between the wheels and the rail are modeled as a linear spring. While m_c is mass of the car body, m_b is mass of the bogie frame, m_w is mass of the wheelset, J_{cy} is moment of inertia of the car body around y axis, J_{cx} is moment of inertia of the car body around x axis, J_{by} is moment of inertia of the bogie around y axis, J_{bx} is moment of inertia of the bogie around x axis, J_{wx} is moment of inertia of the wheelset around x axis, L is length of the car body, L_b is half distance between two bogies, L_c is longitudinal position of the center of the car body, L_f is longitudinal position of the front secondary suspension on the car body, L_r is longitudinal position of the rear secondary suspension on the car body, L_w is half distance between two wheelsets of the bogie, b is lateral displacement of the secondary suspension, b_w is half of the track gauge, k_p is vertical stiffness of the primary suspension per axle box, c_p is vertical damping of the primary suspension per axle box, k_s is vertical stiffness of the secondary suspension for each side of the bogie, c_s is vertical damping of the secondary suspension for each side of the bogie and k_{hz} is equivalent linear spring of the Hertzian contact, ζ_{1z} and ζ_{2z} are the damping coefficients for the first and the second flexible bending modes, respectivelly, $\zeta_{1\phi}$ is the damping coefficient for the first torsional mode. Considering the model shown in Figure 1, the equations of motion of the car body can be written as follows:

$$m_c\ddot{z_c} = -f_{sfr} - f_{sfl} - f_{srr} - f_{srl} \tag{6}$$

$$I_{cy}\ddot{\theta}_c = L_b f_{sfr} + L_b f_{sfl} - L_b f_{srr} - L_b f_{srl} \tag{7}$$

$$I_{cx}\ddot{\phi}_c = -b f_{sfr} + b f_{sfl} - b f_{srr} + b f_{srl} \tag{8}$$

where f_{sij} are related to the secondary suspension forces between bogie frames and the car body. The equations that define these forces are:

$$
\begin{aligned}
f_{sfr} &= k_s[(z_c + \sum X_{nz}(L_f)q_{nz} - L_b\theta_c + b(\phi_c + \sum X_{n\phi}(L_f)q_{n\phi})) - (z_{bf} + b\phi_{bf})] \\
&+c_s[(\dot{z}_c + \sum X_{nz}(L_f)\dot{q}_{nz} - L_b\dot{\theta}_c + b(\dot{\phi}_c + \sum X_{n\phi}(L_f)\dot{q}_{n\phi})) - (\dot{z}_{bf} + b\dot{\phi}_{bf})] \\
f_{sfl} &= k_s[(z_c + \sum X_{nz}(L_f)q_{nz} - L_b\theta_c - b(\phi_c + \sum X_{n\phi}(L_f)q_{n\phi})) - (z_{bf} - b\phi_{bf})] \\
&+c_s[(\dot{z}_c + \sum X_{nz}(L_f)\dot{q}_{nz} - L_b\dot{\theta}_c - b(\dot{\phi}_c + \sum X_{n\phi}(L_f)\dot{q}_{n\phi})) - (\dot{z}_{bf} - b\dot{\phi}_{bf})] \\
f_{srr} &= k_s[(z_c + \sum X_{nz}(L_r)q_{nz} + L_b\theta_c + b(\phi_c + \sum X_{n\phi}(L_r)q_{n\phi})) - (z_{br} + b\phi_{br})] \\
&+c_s[(\dot{z}_c + \sum X_{nz}(L_r)\dot{q}_{nz} + L_b\dot{\theta}_c + b(\dot{\phi}_c + \sum X_{n\phi}(L_r)\dot{q}_{n\phi})) - (\dot{z}_{br} + b\dot{\phi}_{br})] \\
f_{srl} &= k_s[(z_c + \sum X_{nz}(L_r)q_{nz} + L_b\theta_c - b(\phi_c + \sum X_{n\phi}(L_r)q_{n\phi})) - (z_{br} - b\phi_{br})] \\
&+c_s[(\dot{z}_c + \sum X_{nz}(L_r)\dot{q}_{nz} + L_b\dot{\theta}_c - b(\dot{\phi}_c + \sum X_{n\phi}(L_r)\dot{q}_{n\phi})) - (\dot{z}_{br} - b\dot{\phi}_{br})]
\end{aligned}
\tag{9}
$$

where

$$
\ddot{q}_{nz} + 2\zeta_{nz}\omega_{nz}\dot{q}_{nz} + \omega_{nz}^2 q_{nz} = \frac{2}{\rho AL}[-f_{sfr}X_{nz}(L_f) - f_{sfl}X_{nz}(L_f) - f_{srr}X_{nz}(L_r) - f_{srl}X_{nz}(L_r)] \tag{10}
$$

$$
\ddot{q}_{n\phi} + 2\zeta_{n\phi}\omega_{n\phi}\dot{q}_{n\phi} + \omega_{n\phi}^2 q_{n\phi} = \frac{2}{\rho JL}[-bf_{sfr}X_{n\phi}(L_f) + bf_{sfl}X_{n\phi}(L_f) - bf_{srr}X_{n\phi}(L_r) + bf_{srl}X_{n\phi}(L_r)] \tag{11}
$$

The equations of motion for the bogie frame are:

$$
m_b\ddot{z}_{bi} = f_{sir} + f_{sil} - f_{pifr} - f_{pifl} - f_{pirr} - f_{pirl} \tag{12}
$$

$$
I_{by}\ddot{\theta}_{bi} = L_w f_{pifr} + L_w f_{pifl} - L_w f_{pirr} - L_w f_{pirl} \tag{13}
$$

$$
I_{bx}\ddot{\phi}_{bi} = bf_{sir} - bf_{sil} - bf_{pifr} + bf_{pifl} - bf_{pirr} + bf_{pirl} \tag{14}
$$

where f_{pjkl} are related to the primary suspension forces between bogie frames and axle boxes. They are defined in equation (15), where j index should be replaced by f or r to obtain the front or rear bogie primary suspension forces, respectively.

$$
\begin{aligned}
f_{pifr} &= k_p[(z_{bi} - L_w\theta_{bi} + b\phi_{bi}) - (z_{wif} + b\phi_{wif})] + c_p[(\dot{z}_{bi} - L_w\dot{\theta}_{bi} + b\dot{\phi}_{bi}) - (\dot{z}_{wif} + b\dot{\phi}_{wif})] \\
f_{pifl} &= k_p[(z_{bi} - L_w\theta_{bi} - b\phi_{bi}) - (z_{wif} - b\phi_{wif})] + c_p[(\dot{z}_{bi} - L_w\dot{\theta}_{bi} - b\dot{\phi}_{bi}) - (\dot{z}_{wif} - b\dot{\phi}_{wif})] \\
f_{pirr} &= k_p[(z_{bi} + L_w\theta_{bi} + b\phi_{bi}) - (z_{wir} + b\phi_{wir})] + c_p[(\dot{z}_{bi} + L_w\dot{\theta}_{bi} + b\dot{\phi}_{bi}) - (\dot{z}_{wir} + b\dot{\phi}_{wir})] \\
f_{pirl} &= k_p[(z_{bi} + L_w\theta_{bi} - b\phi_{bi}) - (z_{wir} - b\phi_{wir})] + c_p[(\dot{z}_{bi} + L_w\dot{\theta}_{bi} - b\dot{\phi}_{bi}) - (\dot{z}_{wir} - b\dot{\phi}_{wir})]
\end{aligned}
\tag{15}
$$

The equations of motion for the wheelsets are:

$$
m_w\ddot{z}_{wij} = f_{pijr} + f_{pijl} - (N_r + N_l)_{wij} \tag{16}
$$

$$
I_{wx}\ddot{\phi}_{wij} = bf_{pijr} - bf_{pijl} - b_w(N_r - N_l)_{wij} \tag{17}
$$

Similar to equation (15), in equations (16) and (17) the indexes i, j should be replaced by f, r to obtain equation of each front or rear wheelset or bogie, respectively. For example, $\ddot{z}_{wfr}$ is related to the rear wheelset of the front bogie. Moreover, N_r, N_l are normal contact forces between the right wheel and left wheel and rail, respectively. These normal contact forces are defined in equation (18).

$$
\begin{aligned}
N_r &= k_{hz}\delta_r, \quad \delta_r = z_w + b_w\phi_w - z_{0r} \\
N_l &= k_{hz}\delta_l, \quad \delta_l = z_w - b_w\phi_w - z_{0l}
\end{aligned}
\tag{18}
$$

3. Frequency domain analysis

The linear system of equations defined in the previous section can be written in the matrix form as $\mathbf{M}\ddot{X} + \mathbf{C}\dot{X} + \mathbf{K}X = \mathbf{D}Z_0$, where $\mathbf{M}$, $\mathbf{C}$, and $\mathbf{K}$ are mass, damping, and stiffness matrices of the system. Moreover,

D is the stiffness matrix associated with the track excitation. Therefore, the matrix of the frequency response function of the system can be obtained by using equations (19) and (20) [17].

$$\mathbf{H}(\omega) = \left(-\mathbf{M}\omega^2 + j\omega\mathbf{C} + \mathbf{K}\right)^{-1} \tag{19}$$

$$\mathbf{H}_d(\omega) = \mathbf{H}(\omega)\mathbf{D} \tag{20}$$

Thus, the power spectral density associated with the displacements of the system can be obtained by using equation (21):

$$S_{Oi}(\omega) = \sum_{r=1}^{8}\sum_{s=1}^{8} \mathbf{H}^*_{dir}(\omega)\mathbf{S}_{Irs}(\omega)\mathbf{H}^{\mathrm{T}}_{dis}(\omega) \tag{21}$$

where $S_I(\omega)$ is the matrix of the power spectral density of the input excitation. The schematic for the input excitation is presented in Figure 2.

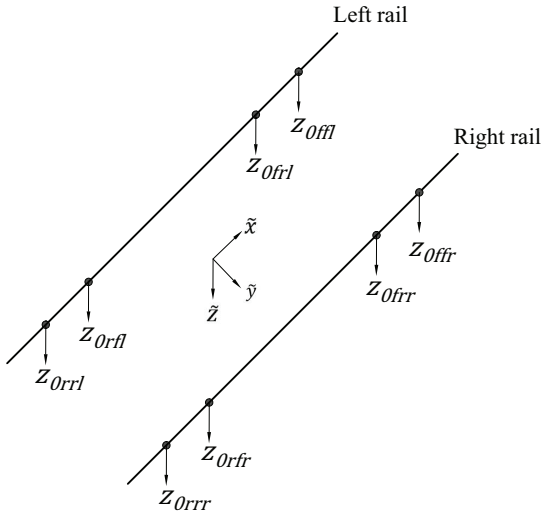

Fig. 2: Track input excitation at the wheel-rail contact point.

According to [25, 26], the torsional irregularity (cross-level) and the vertical irregularity (elevation) at the center of the track are defined as in equation (22).

$$\begin{aligned} \frac{Z_r + Z_l}{2} &= Z_v \\ \frac{Z_r - Z_l}{2} &= Z_c \end{aligned} \tag{22}$$

With the following assumptions, autocorrelation and cross-correlation of the above inputs can be obtained:

- All irregularities are a stationary random process with zero average.
- The irregularity probability density is Gaussian.
- Spectral density is defined in a range of wavelength from 3 to 30m.
- The cross-correlation between different irregularities is zero.

Therefore, according to the auto correlation definition, it is possible to obtain the autocorrelation and the input power spectral density of the irregularities seen by each wheel as expressed in equation (23).

$$\begin{aligned} R_i(\tau) = E[Z_i(t)Z_i(t+\tau)] = E[Z_v(t) + Z_c(t)Z_v(t+\tau) + Z_c(t+\tau)] = \\ E[Z_v(t)Z_v(t+\tau)] + E[Z_v(t)Z_c(t+\tau)] + E[Z_c(t)Z_v(t+\tau)] + E[Z_c(t)Z_c(t+\tau)] \end{aligned} \tag{23}$$

Therefore, the autocorrelation of the irregularities associated to each wheel will be defined by equation (24).

$$R_i(\tau) = R_v(\tau) + R_c(\tau) \tag{24}$$

where $R_v(\tau)$ and $R_c(\tau)$ are autocorrelations of vertical and roll of track irregularities, respectively. The power spectral density of the irregularities associated to each wheel can also be obtained in the similar way, as defined by equation (25).

$$S_i(\omega) = S_v(\omega) + S_c(\omega) \tag{25}$$

where $S_v(\omega)$ and $S_c(\omega)$ are the spectral density of the vertical and roll components of track irregularities, respectively. Moreover, one can obtain the cross-correlation and the cross-spectral density for the left and right wheel associated irregularities from the same wheelset.

$$R_{RLi}(\tau) = R_v(\tau) - R_c(\tau) \tag{26}$$

$$S_{RLi}(\omega) = S_v(\omega) - S_c(\omega) \tag{27}$$

Then, it becomes possible to obtain the input cross-spectral density of the irregularity associated to different wheels in relation to each other. In the case where both wheels are on the same rail, the cross-spectral density function of their input is defined by equation (28).

$$S_{ij}(\omega) = S_i(\omega)e^{-j\omega\left(x_j - x_i\right)/v} \tag{28}$$

In the case where two wheels are not on the same rail, their input cross-spectral density function is as presented in Eq. (29).

$$S_{RiLj}(\omega) = S_{RLi}(\omega)e^{-j\omega\left(x_j - x_i\right)/v} \tag{29}$$

The spectral density functions for vertical and roll components of track irregularity according to the FRA standard [25, 26] is defined by equations (30) and (31).

$$S_v(\Omega) = \frac{A_v\Omega_2^2(\Omega^2 + \Omega_1^2)}{\Omega^4(\Omega^2 + \Omega_2^2)} \tag{30}$$

$$S_c(\Omega) = \frac{A_c\Omega_2^2}{(\Omega^2 + \Omega_1^2)(\Omega^2 + \Omega_2^2)} \tag{31}$$

The rest of the parameters appearing in equations (30) and (31) for a track with classification 6 are defined in Table 1.

Table 1: Parameters of the PSD model for a class 6 track based on FRA standard [25, 26].

A_v (m^3)	A_c (m^3)	Ω_1 (cycle m^{-1})	Ω_2 (cycle m^{-1})
0.98×10^{-8}	0.59×10^{-8}	23.3×10^{-3}	13.1×10^{-2}

FRA: Federal Railroad Administration; PSD: Power Spectral Density.

4. Results and discussion

4.1. Numerical validation of the model

Using equation (21) and the parameters in Table 1, the frequency response of the system can be calculated in the presence of the random uneven track profiles defined in the previous section. Meanwhile, it needs to be reminded that there is no detailed information on Shinkansen's (series 100) elastic vibration characteristics. Also, the modal damping values that are obtained in practice are largely affected by the conditions of the excitation condition. To add to the complexity, the excitation condition through the stationary vibration test that is used to investigate the modal vibration characteristics is completely different from the running situation that is subjected to the displacement excitations from the 8 wheels of the vehicle. Therefore, it is believed that the detailed discussion regarding the modal damping, when the excitation conditions are different, becomes less attractive. An estimation for the damping values for the car body of a commuter train is reported by Tomioka (2012)[27]. Based on the reported experiences, the damping coefficients for the first and the second flexible

bending modes for this research are obtained through a try-error procedure. This included searching for the best fit of the modeling results to the reported measured data by Tomioka (2010)[15]. This resulted in the damping coefficients for the first and the second bending modes equal to 0.012 and 0.003, respectively. Also, the damping coefficient for the flexible twisting mode is equal to 0.011 that is directly taken from Tomioka (2012)[27].

The results presented in this section are obtained by considering a train speed of 300 km/h. Figure 3 compares

Table 2: Technical specification of the Shinkansen vehicle [15].

Parameters	Value	Unit
m_c	16900	kg
m_b	2580	kg
m_w	1510	kg
J_{cy}	$2.1{\cdot}10^6$	kg m^2
J_{cx}	$2.32{\cdot}10^4$	kg m^2
J_{by}	2340	kg m^2
J_{bx}	1580	kg m^2
J_{wx}	1140	kg m^2
L	24.5	m
L_b	17.5	m
L_c	12.25	m
L_f	21	m
L_r	3.5	m
L_w	1.25	m
b	2.2	m
b_w	0.7175	m
k_p	$9.85{\cdot}10^5$	N m^{-1}
c_p	$3.92{\cdot}10^4$	Ns m^{-1}
k_s	$1.28{\cdot}10^6$	N m^{-1}
c_s	$2.255{\cdot}10^4$	Ns m^{-1}
k_{hz}	752	kN mm^{-1}
ζ_{1z}	0.012	-
ζ_{2z}	0.003	-
$\zeta_{1\phi}$	0.011	-

the simulation results for the vertical acceleration at the center of the car body floor with running test which was reported by Tomioka and Takigami [15]. It is observed that at the frequency of 9 Hz the first bending flexural mode appears in both results. While, the second bending flexural mode does not appear. This is because in the center of the car body the related mode shape is nil.

Figure 4 presents the simulation and the running test [15] results of the vertical acceleration at the top of the front bogie of the car body. The second bending flexural mode of the car body appears at 15.12 Hz. While the effect of this flexural mode on the vertical acceleration of the car body is obvious, it is not as effective as the first bending flexural mode. This is because of the averaging (or filtering) effect of the vertical track irregularities. As explained in detail by Tomioka and Takigami [15], Zhou et al. [11] and Gong et al. [17], summation of vertical track irregularities becomes zero at some frequencies. This implies that there are some anti-peaks in the PSD of the vertical acceleration of the car body. This effect is called the averaging (or filtering) effect of vertical irregularities. This filtering effect appears in two forms. The first of them is the bogie base filtering effect and the second is the wheel base filtering effect. The related frequencies can be calculated by equations (32) and (33), respectively. For the vehicle model presented in this article the frequencies related to the wheel base averaging effect are 16.67 Hz, 50 Hz, 83.33 Hz, ... and the frequencies related to the bogie base averaging effect are 2.38 Hz, 7.14 Hz, 11.9 Hz, 16.67 Hz, ... for a train speed of 300 km/h.

In fact, in this case, the first frequency of the wheelbase averaging effect (16.67 Hz) and the fourth frequency of the bogie base averaging effect (16.67 Hz) are close to the frequency of the second bending flexural mode.

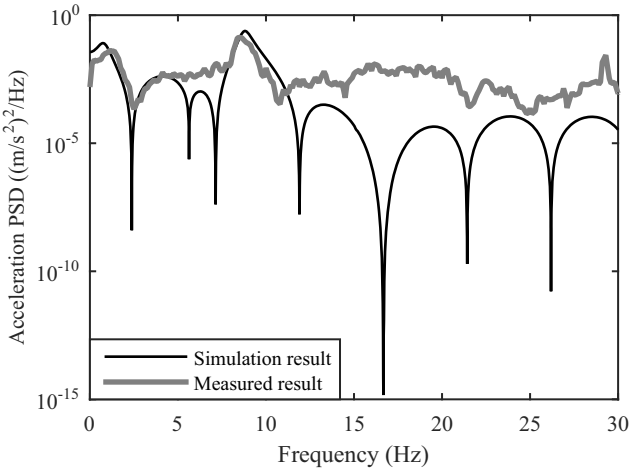

Fig. 3: Comparison between the measured vertical acceleration (running test) at the center of the car body floor reported by Tomioka and Takigami [15] and the simulated frequency response results.

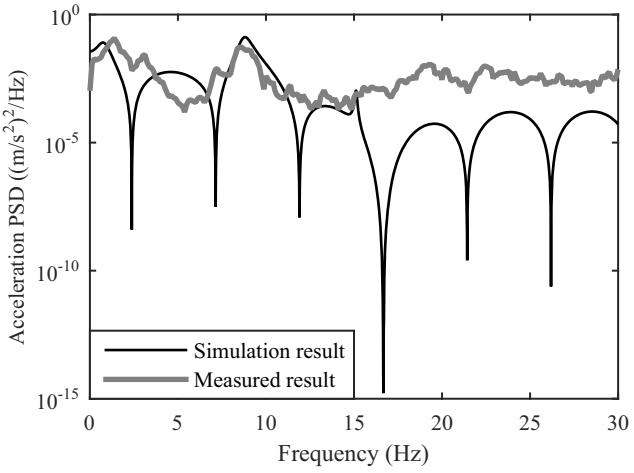

Fig. 4: Comparison between the measured vertical acceleration (running test) at above the front bogie of the car body reported by Tomioka and Takigami [15] and the simulated frequency response results.

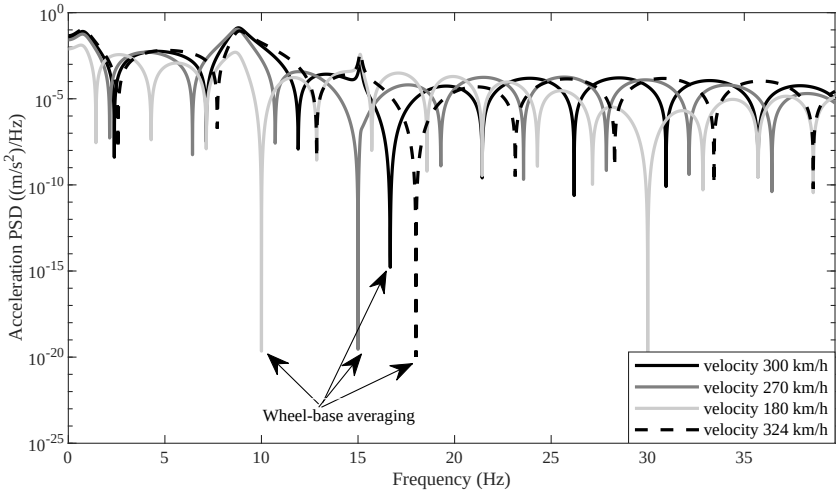

Fig. 5: The averaging frequency effect on the flexible bending modes of the car body.

Therefore, cancellation occurs for this second bending flexural at this specific train speed.

$$f_b = \frac{(2m+1)v}{4L_b}, \quad m = 0, 1, 2, ... \tag{32}$$

$$f_w = \frac{(2n+1)v}{4L_w}, \quad n = 0, 1, 2, ... \tag{33}$$

The calculated vertical acceleration at above the front bogie of the car body for various velocities is presented in Figure 5. The corresponding averaging effect frequencies are calculated by using equations (32) and (33). The results are presented in Table 3. The most important and impressive frequencies for the second bending mode are highlighted in Table 3. They are in close proximity of the carbody 2nd bending mode that appears at 15.12 Hz. Based on the averaging frequency effect that is presented in Figure 5, the effect of wheel-base averaging is higher than the bogie-base averaging. The acceleration associated to the second bending mode frequency at the velocity of 180 km/h is more significant than the related results at the velocities of 270 km/h and 300 km/h. While, the velocity is increased, the vertical acceleration is reduced that is because of the averaging effect. Indeed, for the velocity of 270 km/h, the first wheel-base frequency is near the second bending mode and, as a result, the resulting acceleration is reduced. For the velocity of 300 km/h, the first wheel-base averaging frequency is 16.67 Hz, and there is about 1.5 Hz difference to the second bending mode. However, it has a partial effect on the acceleration associated to the second bending mode. Therefore, this mode isn't entirely canceled by this specific averaging frequency effect. A similar scenario can be explained for the first bending mode. From Figure 5, for the velocity of 180 km/h the first wheel-base frequency is the most important one and, consequently, the relevancy of the first bending mode is reduced remarkably. For the other velocities in this set of results, there isn't any wheel-base averaging frequency near the first bending mode; however, this mode is partially affected by the bogie-base averaging frequency. Indeed, the maximum values of the acceleration associated to the first bending modes did not differ but the bandwidth of the related acceleration is affected. As a result, the ride quality parameter is affected.

Table 3: Averaging frequency effect at various velocities.

	Bogie-base frequency (Hz)							Wheel-base frequency (Hz)		
Velocity (km/h)	1^{st}	2^{nd}	3^{th}	4^{th}	5^{th}	6^{th}	7^{th}	1^{st}	2^{nd}	3^{th}
324	2.57	7.71	12.85	**18**	23.14	28.27	33.41	**18**	54	90
300	2.38	7.14	11.9	**16.67**	21.42	26.18	30.95	**16.67**	50	83.33
270	2.14	6.42	10.71	**15**	19.26	23.54	27.82	**15**	45	75
180	1.42	4.28	7.14	10	12.85	**15.71**	18.46	10	30	50

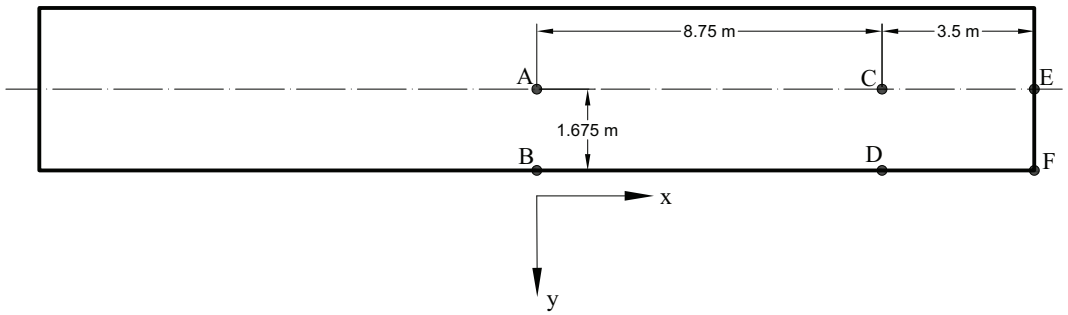

Fig. 6: Top view of the car body and the points where accelerations are studied.

4.2. Effects of the torsional and flexural modes

In this section, the effect of the bending and torsional modes on the dynamic response of the vehicle is investigated. In order to do so, the car body acceleration at locations far from the center of the car body floor is computed.

Figure 6 presents the locations of these points that are all placed on the floor of the car body. Points A, C, and E are located on the car body centerline. With point A positioned at car body center, point C positioned on top of the bogie and point E positioned at the end of the car body. Points B, D and F are located similarly on the car body side wall. Figures 7 and 8 illustrate the simulated vertical acceleration of the car body at such points.

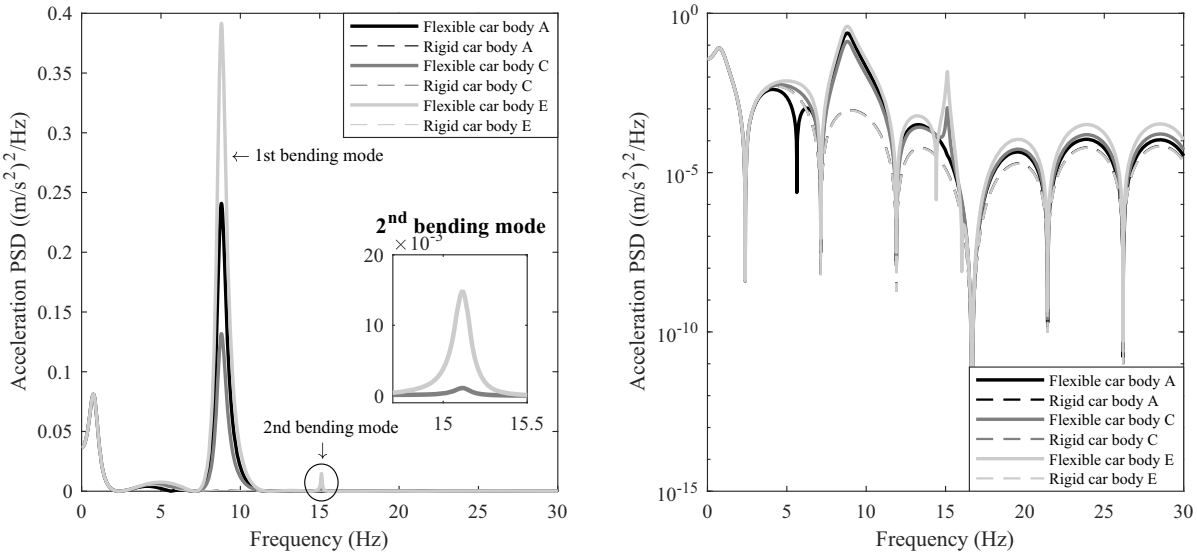

Fig. 7: Power spectral density of the vertical acceleration of the car body at points A, C and E. Linear (left) and logarithmic (right) scale plots.

In Figure 7, at points C and E the second bending flexural mode of the car body appears in the vertical acceleration, while at point A this mode does not appear. This is because the second mode shape of a free-free beam at this point is zero. The ride quality index is the integral of the PSD of the vertical acceleration that in this case is calculated for the frequency range of 4 Hz and 20 Hz [2]. As a resulr, Figure 7 presents that the first bending flexural mode has the highest influence on the ride quality of the vehicle. The previous studies have also pointed to the same issue. However, the torsional flexural effect of the car body on the vertical acceleration is not reported in the previous studies. Figure 8 presents the vertical acceleration of the three points near the car body side wall. These are the points closer to the placements of the passenger sits. As presented, specifically at points D and F the torsional flexible modes of the car body have a significant effect on its vertical acceleration, particularly in the 9 Hz to 15 Hz. This can deteriorate the ride quality index. In other words, in places other than the car body center, and particularly on the sides, the torsional flexural modes can affect the ride quality parameters adversely.

An important factor that can affect the simulation results is the correlation between the irregularities of the

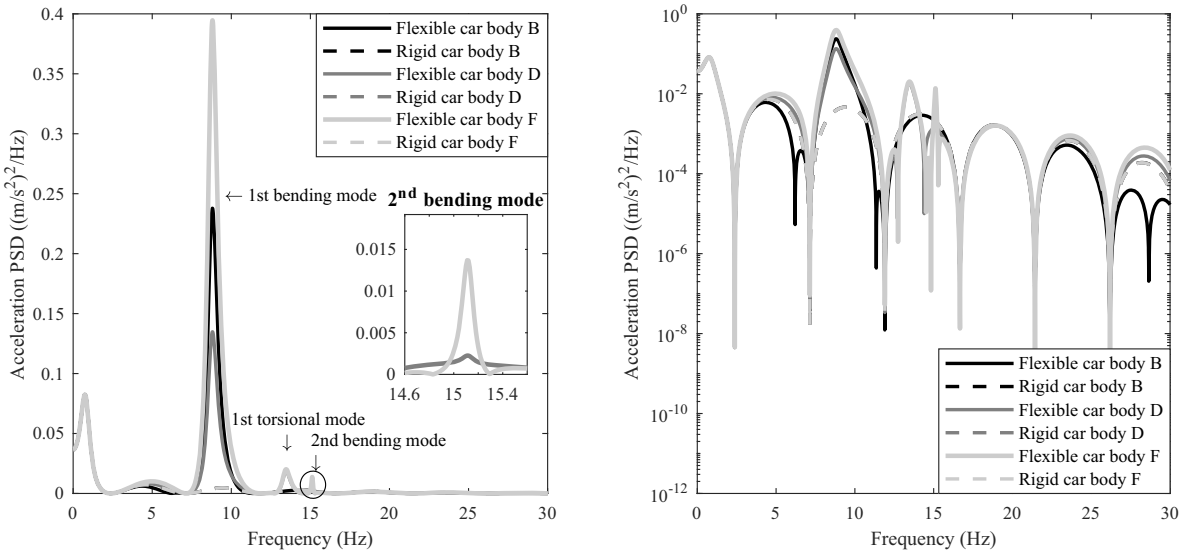

Fig. 8: Power spectral density of the vertical acceleration of the car body at points B, D and F. Linear (left) and logarithmic (right) scale plots.

right and the left rails. Based on the measurements, the vertical irregularities of the right and the left rails are correlated in case of wavelengths longer than 3 m [28]. It means that for a high-speed train at the speed 300 km/h the above-mentioned irregularities are correlated for frequencies smaller than 27 Hz. In order to investigate the degree of correlation of the rail unevenness, three kinds of unevenness 3 types of uneven correlation models are considered. These include completely correlated irregularities, completely uncorrelated irregularities and partially correlated irregularities. The track classification 6 of the FRA is used. Figure 9 presents the coherence between the right and left rail vertical irregularities for the said correlation models. For the completely uncorrelated case it is considered that the correlation between the two rails is equal zero. It means that the elements related to the cross-spectral density between two rails in the input matrix S_{Irs} in equation (21) are zero. For the completely correlated case these elements are exactly the same. In case of partially correlated rail irregularities these elements are defined based on equations (30) and (31).

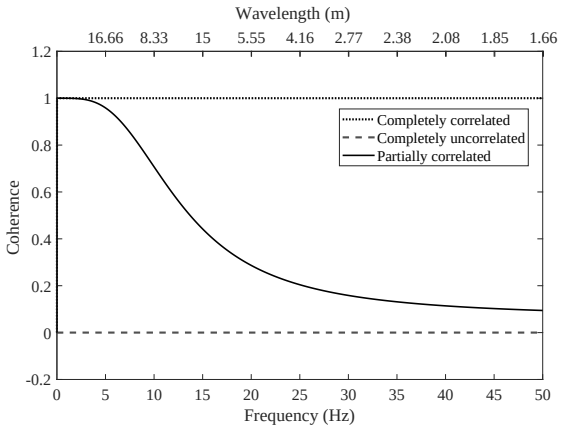

Fig. 9: Coherence between the right and the left rails vertical irregularities.

Figure 10 presents the angular acceleration associated to the roll motion at point C. It is observed that when the irregularities between the two rails are completely correlated, the torsional flexural mode is not significant for the response of car body. On the other hand, when the irregularities are completely uncorrelated or partially correlated, the torsional flexural mode is excited and is relevant in the response. Figure 11 presents the vertical acceleration at points D and F. It is observed that for completely correlated rail irregularities the torsional flexural and the second bending flexural modes are not relevant in the response, while for completely uncorrelated and partially correlated irregularities these modes are significant. Figures 10 and 11 present that the excitation of the torsional flexural mode is strongly affected by the kind of irregularity correlation between the two rails. If the excitation is uncorrelated, the torsional flexural mode is not excited. From the point of view of the flexural bending modes, the correlation model where the excitation seen by these modes is maximum is the completely correlated one. This is because, in this case, the excitation seen by these modes is exactly the double of the

one induced by one rail. In other correlation models, the excitation turns to be less than the double of the rail irregularity and generates a lower response of the system. These are presented in Figures 10 and 11.

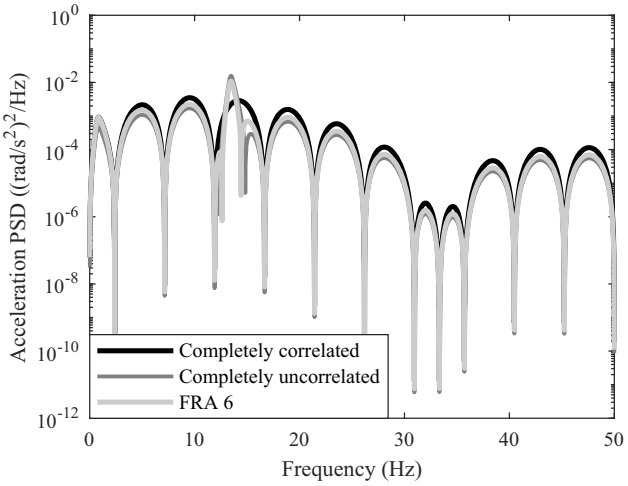

Fig. 10: The effect of the irregularities correlation between the right and the left rails irregularities on roll acceleration for the three rail unevenness correlation models defined at point C.

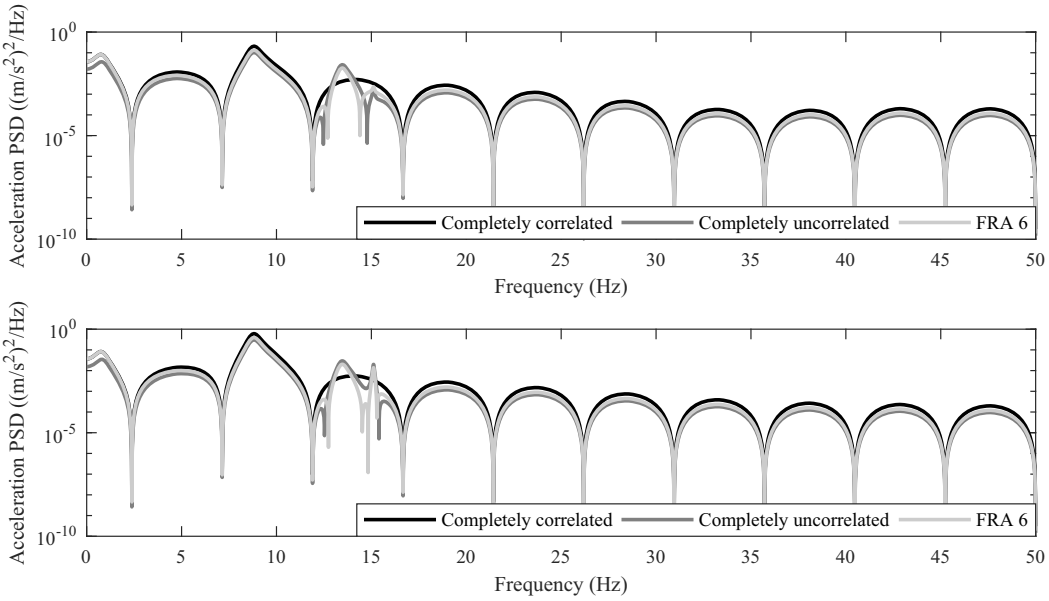

Fig. 11: The effect of the irregularities correlation between the right and the left rails irregularities on vertical acceleration at points D (upper figure) and F (lower figure) of car body.

4.3. Ride quality index assessment

In this section, the ride quality index is calculated based on the EN 12299:2009 [2] standard for various vehicle speeds. The ride quality indexes are calculated for points A, B, C, D, E and F for both rigid and flexible car body. The results are presented in Figure 12. As presented, the ride quality index is not affected significantly by flexural modes for the velocities between 140 to 230 km/h. This is because these modes are not been significantly excited in the said range of speed. However, for a train speed higher than 230 km/h the effect of bending modes on ride quality ibdes becomes clear. The worst train speed for its ride qualityturns to be 298.8 km/h, where the ride quality index increased about 2.2 times when compared with the ride index for the rigid car body at point E. However, it should be noted that the results in Figure 12 are due only to the effect of bending modes. The effect of torsional mode do not appear at the selected points (A, B, C) in the car body floor. In Figure 13 the calculated ride indexes on points B, D and F are presented. The eefect of tosional vibration mode on the ride quality index in points D and F is obvoius. In point B that coincides with a vibration node the first torsional flexural mode is not effective. In contrast, in points D and F the effect of the torsional flexural mode is clear that adds to the effect of the first and the second bending modes. For example, at the train speed of

298.8 km/h the ride index for the flexible car body is 70 % more when compared with a rigid car body model at point F. In this case the ride quality index increased from 0.681 to 1.162.

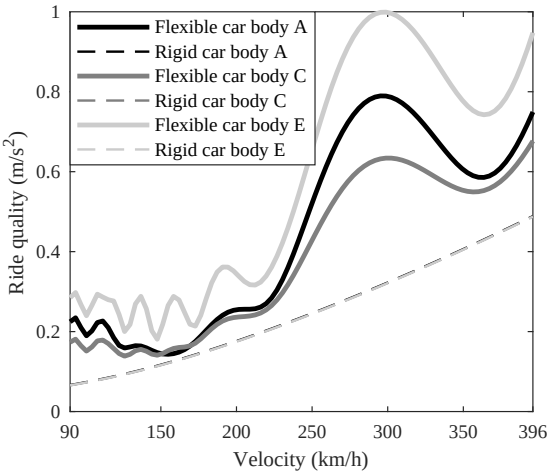

Fig. 12: The effect of vehicle velocity on the vertical ride quality at points A, C and E of car body.

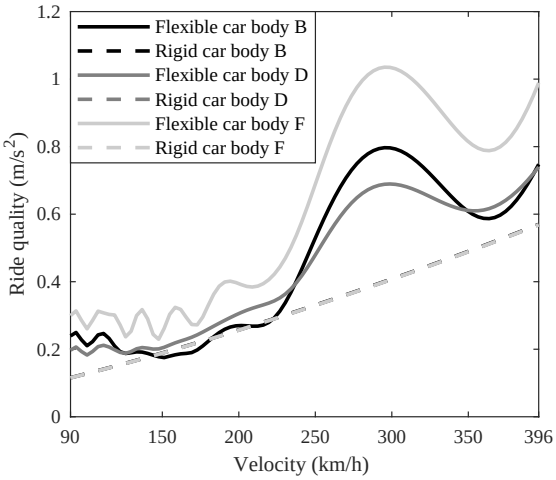

Fig. 13: The effect of vehicle velocity on the vertical ride quality at points B, D and F of car body.

Figure 14 presents a comparison for the effects due to the rigid roll motion and bending and torsional flexural modes on the vertical ride quality at point F. It is observed that the rigid roll acceleration of the car body has a notable effect on the vertical ride quality so that this index becomes about 10 % higher for any train speed. In contrast, the torsional flexural mode has a negative effect on the vertical ride quality only at some specific speeds. Indeed, the filtering effect of the vertical track irregularities is not able to cancel the effect of the torsional flexural mode for speeds of 200 km/h and 290 km/h. Thus, the ride quality index become higher at such speeds of travel.

Figure 15 presents the variation of the ride quality index versus the train speed for different types of correlations between the rail irregularities. The correlation model to which the lower vertical ride quality index is associated is the completely uncorrelated rail irregularities. However, it should be noted that, this kind of rail irregularities correlation model is the one that puts more excitation on the torsional flexural mode. This is also clear form the results that are presented in Figure 11. Even so, since the most significant mode in terms of the vertical ride quality is the first bending flexural mode, and by taking into account that this mode is excited by completely correlated irregularities more than the rest of the correlation models, the completely correlated rail irregularities is the worst case in terms of the vertical ride quality. Also, the second point is that the second bending flexural mode does not affect the vertical ride quality index as much as the first bending flexural mode. This is because this mode is not excited by the track irregularities. Furthermore, as is presented in Figure 15 the vertical ride quality indexes are different for rigid modes. It means that the vertical rigid motion related to the secondary suspension system is excited differently according to the kind of irregularities. For the cases of the completely correlated or partially correlated rail irregularities, this rigid mode is excited almost equally. But for the case of

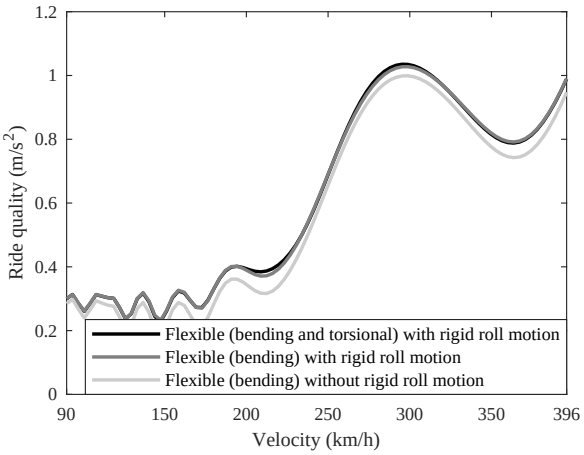

Fig. 14: Ride quality index of the car body at point F against the train speed of travel at various flexibility conditions.

the completely uncorrelated irregularities, the amplitude of the vertical acceleration associated with this rigid mode is smaller than the other kinds of irregularity correlation models.

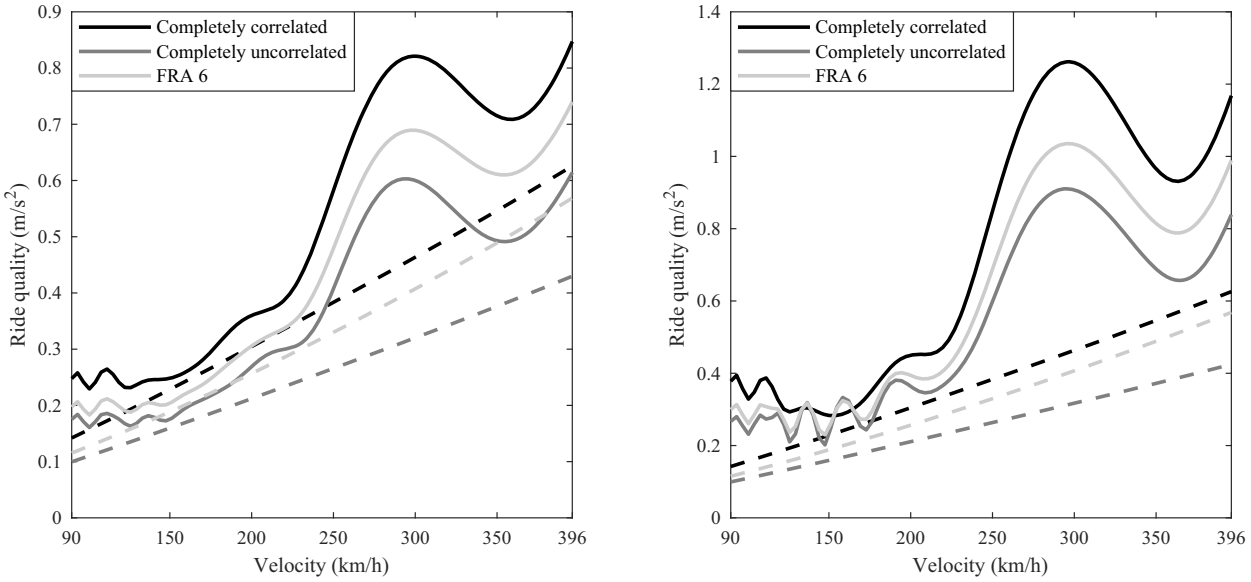

Fig. 15: The effect of correlation between the right and the left rails irregularities on ride quality at points D (left) and F (right) for the case of a flexible model of the car body (continuous line) and the rigid model of the car body (dashed line).

5. Conclusions

It is reported by previous studies that the bending flexural vibration of the car body has a negative effect on the ride quality index of the rail vehicles. But the simultaneous effect of bending and torsional flexural vibration of the car body is not reported. In this study, the combined effect of the bending and torsional flexible modes of the car body on the dynamic response of the vehicle and its ride quality are investigated. A high-speed Shinkansen vehicle with a flexible body is modeled by considering torsional and bending flexural modes and is analyzed in the frequency domain. For this purpose, the rail irregularities are compatible with classification 6 of the FRA regulations. Moreover, three types of irregularity correlation models between the left and the right rails are considered. These include the completely correlated, completely uncorrelated, and partially correlated rail irregularities.

1. It is found that the first bending flexural mode of the car body has a significant effect on the vertical acceleration of the car body floor along the car body centerline. However, the second bending flexural mode is not as important as the first bending flexural mode with respect to the ride quality index.

2. Moving towards the car body wall, the effect of the torsional flexural modes on the vertical acceleration increases, particularly in the frequency range of 4 Hz to 20 Hz. this is the frequency range of interest for the ride quality based on the EN 12299 standard, that can induce an adverse effect on the ride quality parameters. It is also found that the car body vertical acceleration is affected by the torsional flexural mode of the car body in the frequency range of 4 Hz to 20 Hz. The ride quality index in the selected points on the wall of the car body is higher than the points on the center line of the car body. According to the results, in some special velocities the ride quality index increased to two folds. This is because the filtering (or averaging) effect of the vertical irregularity is not able to cancel the effect of the flexural modes of vibration of the car body.

3. Also, it is concluded that the correlation between the right and the left rail irregularities can affect the vertical acceleration hence alters the ride quality index. For example, in the case of completely correlated irregularities, the torsional flexural mode is not excited. In this case the rigid mode of the secondary suspension and the first bending flexural mode are excited more than the completely uncorrelated irregularities. As a result, in such cases, the vertical acceleration at some points on the car body side wall is more dependent on the correlation between the right and the left rail irregularities.

Acknowledgments

The authors would like to express their gratitude to Professor Takahiro Tomioka for his expedient information about the Shinkansen train and his valuable suggestions.

List of Symbols

b lateral displacement of the secondary suspension

b_w half of the track gauge

c_p vertical damping of the primary suspension per axle box

c_s vertical damping of the secondary suspension for each side of the bogie

f_{sij} secondary suspension forces between bogie frames and the car body

f_{pjkl} primary suspension forces between bogie frames and axle boxes

J_{bx} moment of inertia of the bogie around x axis

J_{by} moment of inertia of the bogie around y axis

J_{cx} moment of inertia of the car body around x axis

J_{cy} moment of inertia of the car body around y axis

J_{wx} moment of inertia of the wheelset around x axis

k_{hz} equivalent linear spring of the Hertzian contact

k_p vertical stiffness of the primary suspension per axle box

k_s vertical stiffness of the secondary suspension for each side of the bogie

L length of the car body

L_b half distance between two bogies

L_c longitudinal position of the center of the car body

L_f longitudinal position of the front secondary suspension on the car body

L_r longitudinal position of the rear secondary suspension on the car body

L_w half distance between two wheelsets of the bogie

m_b mass of the bogie frame

m_c mass of the car body

m_w mass of the wheelset

N_l normal contact forces between the left wheel of each wheelset and rail

N_r normal contact force between the right wheel of each wheelset and rail

v vehicle velocity

ζ_{1z} damping coefficient for the first flexible bending mode

ζ_{2z} damping coefficient for the second flexible bending mode

$\zeta_{1\phi}$ damping coefficient for the first flexible torsional mode

[1] T. Takigami, T. Tomioka, Modal vibration analysis of recent railway vehicles, in: Proceedings of the 12th Asia Pacific Vibration Conference (APVC2007), 2007, pp. 6–9.

[2] EN 12299:2009, Railway applications-Ride comfort for passengers -Measurement and evaluation, Standard, British Standard, Brussels, 2009.

[3] G. Capitani, M. Tibaldi, Reduced-order controllers for active suspension of vehicles with flexible body, IMAGS Conference (1989) 201–6.

[4] A. Hac, I. Youn, H. H. Chen, Control of suspensions for vehicles with flexible bodies—part i: active suspensions, Journal of dynamic systems, measurement, and control 118 (1996) 508–17.

[5] E. Foo, R. Goodall, Active suspension control of flexible-bodied railway vehicles using electro-hydraulic and electro-magnetic actuators, Control Engineering Practice 8 (2000) 507–18.

[6] P. Carlbom, Carbody and passengers in rail vehicle dynamics, Ph.D. thesis, Institutionen för farkostteknik, 2000.

[7] J. Hansson, M. Takano, T. Takigami, T. Tomioka, Y. Suzuki, Vibration suppression of railway car body with piezoelectric elements, JSME International Journal Series C Mechanical Systems, Machine Elements and Manufacturing 47 (2004) 451–6.

[8] T. Takigami, T. Tomioka, Bending vibration suppression of railway vehicle carbody with piezoelectric elements, Journal of Mechanical Systems for Transportation and Logistics 1 (2008) 111–21.

[9] G. Schandl, P. Lugner, C. Benatzky, M. Kozek, A. Stribersky, Comfort enhancement by an active vibration reduction system for a flexible railway car body, Vehicle System Dynamics 45 (2007) 835–47.

[10] A. Schirrer, M. Kozek, Co-simulation as effective method for flexible structure vibration control design validation and optimization, in: Control and Automation, 2008 16th Mediterranean Conference on, IEEE, 2008, pp. 481–6.

[11] J. Zhou, R. Goodall, L. Ren, H. Zhang, Influences of car body vertical flexibility on ride quality of passenger railway vehicles, Proceedings of the Institution of Mechanical Engineers, Part F: Journal of Rail and Rapid Transit 223 (2009) 461–71.

[12] Y. Sugahara, T. Takigami, R. Koganei, Suppression of vertical bending vibration in railway car bodies by primary suspension damping control (results of running tests using shinkansen vehicles), in: Proceedings of the International Symposium on Dynamics of Vehicles on Roads and Tracks (IAVSD'09), Stockholm, Sweden, 2009.

[13] Y. Sugahara, A. Kazato, R. Koganei, M. Sampei, S. Nakaura, Suppression of vertical bending and rigid-body-mode vibration in railway vehicle car body by primary and secondary suspension control: results of simulations and running tests using shinkansen vehicle, Proceedings of the Institution of Mechanical Engineers, Part F: Journal of Rail and Rapid Transit 223 (2009) 517–31.

[14] A. Orvnäs, Methods for reducing vertical carbody vibrations of a rail vehicle: a literature survey, KTH, 2010.

[15] T. Tomioka, T. Takigami, Reduction of bending vibration in railway vehicle carbodies using carbody–bogie dynamic interaction, Vehicle System Dynamics 48 (2010) 467–86.

[16] T. Kamada, K. Hiraizumi, M. Nagai, Active vibration suppression of lightweight railway vehicle body by combined use of piezoelectric actuators and linear actuators, Vehicle system dynamics 48 (2010) 73–87.

[17] D. Gong, J.-s. Zhou, W.-j. Sun, On the resonant vibration of a flexible railway car body and its suppression with a dynamic vibration absorber, Journal of Vibration and Control 19 (2013) 649–57.

[18] J. L. Escalona, H. Sugiyama, A. A. Shabana, Modelling of structural flexiblity in multibody railroad vehicle systems, Vehicle System Dynamics 51 (2013) 1027–58.

[19] W. Sun, J. Zhou, D. Gong, T. You, Analysis of modal frequency optimization of railway vehicle car body, Advances in Mechanical Engineering 8 (2016) 1687814016643640.

[20] M. Graa, M. Nejlaoui, A. Houidi, Z. Affi, L. Romdhane, Development of a reduced dynamic model for comfort evaluation of rail vehicle systems, Proceedings of the Institution of Mechanical Engineers, Part K: Journal of Multi-body Dynamics 230 (2016) 489–504.

[21] M. Masoomi, M. M. Jalili, Non-linear vibration analysis of a 2-dof railway vehicle model under random rail excitation, Proceedings of the Institution of Mechanical Engineers, Part K: Journal of Multi-body Dynamics 231 (2017) 591–607.

[22] M. Dumitriu, Ride comfort enhancement in railway vehicle by the reduction of the car body structural flexural vibration, in: IOP Conference Series: Materials Science and Engineering, volume 227, IOP Publishing, 2017, p. 012042.

[23] C. Huang, J. Zeng, G. Luo, H. Shi, Numerical and experimental studies on the car body flexible vibration reduction due to the effect of car body-mounted equipment, Proceedings of the Institution of Mechanical Engineers, Part F: Journal of Rail and Rapid Transit 232 (2018) 103–20.

[24] A. W. Leissa, M. S. Qatu, Vibrations of Continuous Systems., McGraw-Hill, 2011.

[25] L. Frỳba, Dynamics of railway bridges, Thomas Telford Publishing, 1996.

[26] D. GargVK, Dynamicsofrailwayvehiclesystems, Or land, USA: AcademicPress (1984).

[27] T. Tomioka, T. Takigami, K. Aida, Modal vibration characteristics of flexural vibrations in railway vehicle carbodies, in: Proceedings of the First International Conference on First International Conference on Railway Technology: Research, Development and Maintenance (Railways 2012), 2012, pp. 18–20.

[28] E. Ntotsios, D. Thompson, M. Hussein, The effect of track load correlation on ground-borne vibration from railways, Journal of Sound and Vibration 402 (2017) 142–63.

List of Figures